Deep learning-aided redesign of a hydrolase for near 100% PET depolymerization under industrially relevant conditions

Bian Wu (wub@im.ac.cn)
Insitute of Microbiology, CAS

Yinglu Cui
State Key Laboratory of Microbial Resources & CAS Key Laboratory of Microbial Physiological and Metabolic Engineering, Institute of Microbiology, Chinese Academy of Sciences https://orcid.org/0000-0002-2147-5879

Yanchun Chen
Institute of microbiology, CAS

Jinyuan Sun
Institute of microbiology, CAS

Tong Zhu
Institute of microbiology, CAS

Hua Pang
Institute of microbiology, CAS

Chunli Li
Institute of microbiology, CAS

Wenchao Geng
Institute of microbiology, CAS

Biological Sciences - Article

Keywords:

Posted Date: January 18th, 2023

DOI: https://doi.org/10.21203/rs.3.rs-2465520/v1

Abstract

Biotechnological plastic depolymerization and recycling have emerged as suitable options for addressing the plastic-waste pollution crisis in a circular plastic economy. Enzymatic degradation of poly(ethylene terephthalate) (PET), as the most typical representative, has evolved over the past two decades, with a major breakthrough achieved by using the LCC variant that permitted 90% conversion of PET on an industrial scale. Despite the achievements, the last 10% residual PET becomes nonbiodegradable due to physical aging, which has hampered its application in real industrial scenarios. In the present study, we addressed current challenges by employing a computational strategy that incorporates a protein language model and force-field-based algorithms to engineer a hydrolase from the bacterium HR29. The redesigned variant, TurboPETase, outperformed all the PET hydrolases reported thus far with regard to industrial application, enabling nearly 100% depolymerization of untreated PET containers, pretreated postconsumer PET bottles and their lower-grade products. The full degradation of pretreated PET at high industrially relevant scales (up to 300 g L-1) can be accomplished in as little as 10 h, with a maximum production rate of 77.3 gTPAeq L 1 h-1, demonstrating great potential for enzymatic PET recycling. Kinetic parameters derived from the inverse Michaelis–Menten model and structural analysis suggest that the improved depolymerization performance may be attributed to a more flexible PET-binding groove that facilitates the targeting of more specific attack sites. Collectively, our results constitute a significant advance in the understanding and engineering of effective industrially applicable polyester hydrolases and provide guidance for further efforts on other mass-produced polymer types in this intriguing research field.

Main

Earth's ecosystem is approaching a planetary-scale transformation as a result of human influence[1]. A wide variety of petroleum-based synthetic polymers are produced worldwide, with a 20-fold increase in annual production since the 1960s, and a slowdown of this trend is not expected[2]. Marine pollution and the negative impacts of microplastic exposure on human health have caused escalating public and governmental concerns, boosting the demand for a circular plastic economy[3-7]. In this regard, biotechnological plastic recycling has become a thriving research area in recent years[8-10]. Poly(ethylene terephthalate) (PET) is one of the most widely used man-made synthetic plastics worldwide, with an annual manufacturing capacity of over 30 million tons[2]. Over the past two decades, research on the biodegradation of PET has progressed from detection of trace amounts of released products to highly efficient degradation[11-12]. A breakthrough was achieved in 2020 with the development of an engineered LCC variant (LCC^{ICCG}) that exhibited 90% depolymerization of pretreated PET waste at high PET concentrations (200 g kg^{-1}). Further synthesis of virgin polymers by using the released monomers offered a glimpse into the application of biocatalysis in plastic recycling at the industrial level[13]. However, the 10% conversion loss due to the nonbiodegradable residual PET waste with a large increase in crystallinity represents an unmet challenge (Fig. 1A). Such limitations can be vastly suppressed by decreasing the reaction temperature, but the catalytic efficiency of PET hydrolases is concomitantly

sacrificed[14], which is not desirable as the reaction duration has a greater impact on the process cost than the energy cost of maintaining elevated operating temperatures[12, 15]. In most homogeneous reactions, high enzyme loading is generally preferred for maximizing reactor productivity. However, as a typical surface erosion process, enzymatic hydrolysis of PET can hardly permeate the inner core of the polymer, resulting in a limited number of superficial ester bonds (also termed attack sites) being accessed even if the enzymes are in great excess[16, 17]. Saturation thus occurs when all attack sites on the surface become occupied, and the excess enzyme molecules accumulate in the solvent (Fig. 1B). Therefore, the desired improvement in depolymerization efficiency can hardly be accomplished by simple process optimization, increasing the demand for new functional enzymes with balanced thermostability and high hydrolytic efficiency.

Previous efforts have been expended in the quest for new PET hydrolases as well as in the optimization of known enzymes[18-22]. A recently reported variant of *Is*PETase using a machine-learning-aided approach (FastPETase) affords improved depolymerization efficiency compared to that of other *Is*PETase mutants at 50 °C[18]. More recently, directed evolution was used to generate HotPETase with a T_m of 82.5 °C, which degrades PET more efficiently than LCC^{ICCG} after 1 h of reaction at low enzyme loading (0.29 $mg_{enzyme}\ g^{-1}$ enzyme loading) at 65 °C[19]. However, in heterogeneous catalysis reactions, different enzymes may exhibit dramatically distinct catalytic efficiencies at low and high enzyme concentrations, as in the case of cellulases[16]. Erickson *et al.* also demonstrated that *Is*PETase showed similar hydrolytic conversion compared to its variant *Is*PETase$^{W159H/S238F}$ at low enzyme loading (0.5-1 $mg_{enzyme}\ g_{PET}^{-1}$), but approximately 2-fold lower conversion at higher enzyme loading (3 $mg_{enzyme}\ g_{PET}^{-1}$)[23]. Since different studies employ varying experimental conditions, the designed PET hydrolases may not maintain their reported catalytic efficiency at the industrial level. Therefore, we evaluated the depolymerization performance of LCC, LCC^{ICCG}, BhrPETase, FastPETase, and HotPETase at various enzyme loading levels, but unfortunately, at enzyme saturation conditions, none of the engineered PET hydrolases tested exhibited higher catalytic performance than LCC^{ICCG} except for BhrPETase, which showed similar hydrolysis efficiency (Fig. 1C).

The last few years have witnessed impressive progress in the tailoring of natural enzymes by computational redesign strategies[24]. Given our limited knowledge of how a sequence encodes catalytic function in polymer-degrading enzymes, exploiting physics-based computational redesign and rational design approaches is suboptimal for improving the interfacial reaction efficiency. Inspired by the achievements in artificial intelligence for addressing the protein fitness landscape to probe hidden evolutionary information, we employed a computational strategy that incorporates a protein language model and force-field-based engineering algorithms to address the aforementioned challenge. The redesigned PET hydrolase (TurboPETase) derived from this campaign exhibited a 4.4-fold improvement in PET-specific activity compared to that of wild-type BhrPETase and LCC^{ICCG} under enzyme saturation conditions. The extraordinary degradation performance afforded by TurboPETase allowed nearly 100% depolymerization toward untreated PET containers in merely one day, as well as the full degradation of

pretreated postconsumer PET bottles and lower-grade PET products at an industrially relevant scale, addressing the challenge with regard to the residual nonbiodegradable PET waste and rendering this highly efficient, optimized enzyme a good candidate for future applications in industrial plastic recycling processes. The mechanism underlying the promotion of enzyme performance has been demonstrated via kinetic analyses derived from an inverse Michaelis–Menten reaction regime as well as structural analysis, highlighting the importance of the ability to target specific attack sites on the polymer surface.

Computational redesign of an efficient PET hydrolase.

Although nature has evolved a family of hydrolases to degrade PET polymers, they share common structural features (a canonical catalytic triad and oxyanion hole) with other esterases that act on small molecules and comparable conversion rates for soluble esters[12]. A quantum mechanics/molecular mechanics (QM/MM) study revealed that the free energy barrier and hydrolytic reaction thermodynamics do not differ significantly between *Is*PETase and the LCC^{ICCG} mutant[25]. Therefore, it is likely that the ability to attach to the PET surface, rather than the core catalytic motif, has been modified during the evolutionary trajectory of hydrolases to enhance the depolymerization of insoluble plastics, as with other natural polymer-degrading enzymes. Describe the mapping from protein sequence to function through deep learning-based models has proven to be successful in many cases[26-28]. Divergence times that indicate the improvement in polymer degradation during evolution may be captured from the relative fitness of variants of a protein along the evolutionary landscape.

To this end, we employed a language model trained on two datasets that involved approximately 26,000 homologous sequences of PET hydrolases and other esterases across evolution, to predict the probability of amino acid variation from the evolutionary landscape (Fig. 2A). BhrPETase and LCC^{ICCG} were used as the inputs due to their relatively high thermostability and hydrolytic activity. A Transformer encoder was used to process input amino acid sequences with absolute position embedding. Residue positions are sorted by the mean of the logits of 19 mutations assigned to the wild type amino acid at each position. The top ten amino acid positions with the highest average scores of each model were selected. After removing duplicated amino acid positions from the 40 top candidates, 18 amino acid positions where the wild-type residues fit less well than potential substitutions were obtained (Supplementary Table S1).

According to the crystal structures of BhrPETase (PDB code: 7EOA) and LCC^{ICCG} S165A in complex with MHET (PDB code: 7VVE[29]), 7 of the 18 generated amino acid positions (W104, H164, M166, W190, H191, H218, and F/I243) were suggested to be embedded in a PET-binding groove (Fig. 2B). Recently, Chen *et al.* reported that the Ser214/Ile218 double mutants of several *Is*PETase-homologous enzymes had enhanced PET hydrolysis activity (by at least 1.3-fold) but vastly decreased T_m values (by approximately 10 °C)[30]. Since His218 (corresponding to Ser214 in *Is*PETase) was involved in our predicted candidates, we initially explored the hydrolytic performance of the H218S/F222I variant on both BhrPETase and LCC^{ICCG}. As expected, BhrPETase$^{H218S/F222I}$ and LCC$^{ICCG/H218S/F222I}$ variants demonstrated a 2.6-fold and 1.9-fold increase in PET-hydrolytic activity, respectively, compared to the wild-type scaffolds in the hydrolysis of

Gf-PET films at 65 °C under enzyme saturation conditions (Supplementary Table S2). In particular, the BhrPETase$^{H218S/F222I}$ variant yielded 1.4-fold greater levels of degradation products than the LCC$^{ICCG/H218S/F222I}$ variant, suggesting that this engineered enzyme is a more suitable candidate for further engineering. Using the BhrPETase$^{H218S/F222I}$ (referred to as BhrPETase M2) variant as the starting point, we subjected the remaining 6 positions (W104, H164, M166, W190, H191 and F243) to generate 32 variants (Supplementary Table S3). After experimental verification, W104L, W104S, W104H, W104G, F243I, F243T, and F243G resulted in improved hydrolytic activities (by 10% to 34%).

Notably, the BhrPETase M2 variant exhibited a melting temperature of 85 °C, which was 11 °C lower than that of the wild-type enzyme. The active mutations at the W104 and F243 positions on BhrPETase M2 reduced the stability even further, with T_m values ranging from 71.5 °C to 84 °C. Empirical data have suggested that an at least 12 °C higher T_m than the T_{opt} is needed to enable catalyst longevity[20]. Hence, a PET hydrolase with a T_m over 77-85 °C is preferred for efficient PET degradation. The nonnegligible decrease in the stability of the active variants limited further combination, and compensatory mutations needed to be introduced first to suppress the deleterious effects. Therefore, we applied our previously devised GRAPE strategy[21], which employs four complementary algorithms, namely, FoldX[31] (force field energy function), Rosetta_cartesian_ddg[32] (force field energy function), ABACUS[33] (statistical energy function) and DDD[34] (force field energy function), to design stabilizing mutations to compensate and buffer the destabilizing mutations (Fig. 2C). Upon experimental validation, 3 beneficial variants (A209R, D238K, and A251C-A281C) resulted in improved thermostability without compromising the activity (Supplementary Table S4). We added the stabilizing variants to BhrPETase M2 using a stepwise combining strategy and resulted in a BhrPETase M6 variant (BhrPETase$^{H218S/F222I/A209R/D238K/A251C/A281C}$), which exhibited a restored melting temperature of 97 °C without sacrificing activity. Subsequently, active mutations at the W104 and F243 positions were combinatorically assembled and accumulated onto the thermostable BhrPETase M6 variant, generating 12 new variants (Fig. 2D). After comparative analysis of specific activities and melting temperatures (Supplementary Table S5), the best combination variant, BhrPETase$^{H218S/F222I/A209R/D238K/A251C/A281C/W104L/F243T}$ (referred to as TurboPETase), was selected with a T_m of 84 °C and a significant 4.4-fold improvement in PET-specific activity towards GF-PET films compared to wild-type BhrPETase.

We subsequently evaluated the depolymerization rate of TurboPETase with respect to other PET hydrolases under enzyme saturation conditions across a range of temperatures from 40 to 72 °C (Supplementary Fig. S1). The degradation results highlight the substantially superior hydrolysis activity performance of TurboPETase at all the temperatures tested, especially at elevated temperatures of 65 °C and 72 °C (Fig. 2E). At 65 °C, BhrPETase, LCC^{ICCG}, HotPETae and FastPETase achieved 5.2%, 5.2%, 2.6%, and 0.6% depolymerization within 3 h, a time course over which the reaction progressed linearly. At the same temperature, TurboPETase afforded 21% depolymerization, which was 4-, 4-, 8- and 33-times higher than those of BhrPETase, LCC^{ICCG}, HotPETae and FastPETase, respectively. At 72 °C, the depolymerization

of TurboPETase was improved to 32% in 3 h, whereas other PET hydrolases reached 0.3%-9% conversion. Even at 50 °C, TurboPETase can achieve 3% depolymerization, which is 1.8-fold higher than that of FastPETase after 3-h reaction. It is worth noting that the higher depolymerization performance was mainly attributed to the specific hydrolysis activity rather than the greater product accumulation during long-term survival due to the enhanced longevity. This is not to say that TurboPETase can not suffer from prolonged periods of elevated temperatures. At 65 °C, extending the incubation time to 24 h accomplished approximately 100% depolymerization, which confirmed the thermotolerance and catalytic performance of TurboPETase.

The successful design encouraged further exploration of the generalizability of the predicted active mutations in other PET hydrolases. The W104L and F243T mutations were introduced to several homologous enzymes, including LCC^{ICCG}, Tfh from *Thermobifida fusca*[35], and Tfcut2 from *T. fusca* KW3[36](Supplementary Fig. S2). To our delight, the resulting W104L variants of LCC^{ICCG}, Tfh (in which the corresponding residue is W109L) and Tfcut2 (in which the corresponding residue is W109L), showed enhanced hydrolytic activity on Gf-PET films (up to a 6.9-fold increase), albeit with reduced thermostabilities relative to those of their respective scaffolds (T_m decreased by 4-6 °C), thus showcasing the portability of this mutation to other PET hydrolases. In contrast to the W104L mutation, the F243T variants of Tfh (in which the corresponding residue is F249T) and Tfcut2 (in which the corresponding residue is F249T) showed no beneficial effect on enzyme activity, suggesting that this mutation may only affect the hydrolytic activity of BhrPETase and its highly homologous proteins.

Mechanism underlying the improved properties of TurboPETase via an inverse Michaelis–Menten approach and structural analysis

The depolymerization performance under enzyme saturation conditions can provide important guidance for further efforts in engineering enzymes for industrial promise. However, in the absence of physically meaningful kinetic parameters, one can typically perform superficial analyses to interpret the molecular mechanisms of the catalytic process. As this is a heterogeneous process, the real accessible molar concentration of the substrate is unknown, which makes the use of textbooks on enzyme kinetics challenging. An inverse Michaelis–Menten equation has been successfully employed to study the kinetics of heterogeneous enzymes such as cellulases, by which the catalytic efficacy against accessible attack sites on the PET surface can be estimated[37-39].

In this study, the kinetic parameters of both the conventional Michaelis–Menten model and inverse Michaelis–Menten model were determined by fitting for several PET hydrolases at 65 °C on Gf-PET films. The conventional Michaelis–Menten model examines reaction regimes in which the substrate is present at substantially higher levels than the biocatalyst, whereas the inverse Michaelis–Menten model studies the reaction with enzyme in excess of the substrate. As shown in Fig. 3A, the curves showed near-linear relationships of the initial rate and substrate load under all conditions for TurboPETase, BhrPETase and LCC^{ICCG}. Conventional saturation behaviour was not observed because even the lowest enzyme concentrations used here (0.12 μM) were too high for the conventional approach to be valid, which

indicates the very fast rates of dissociation of the enzymes from the PET surface. Therefore, increasing the substrate concentration seems to have a marginal effect on conversion yields at the same enzyme/substrate ratio. Further research with more sophisticated techniques is needed to determine the molecular origins of the high $^{conv}K_M$ and $^{conv}V_{max}$ values for these PET hydrolases.

Although these enzymes could not meet the criteria for the conventional approach, the inverse approach was more applicable. The kinetic parameters $^{inv}K_M$ and $^{inv}V_{max}/^{mass}S_0$, derived from the nonlinear regression analyses in Fig. 3B are listed in Table 1. The results for $^{inv}K_M$ in Table 1 revealed marginal differences between TurboPETase, BhrPETase, and LCC^{ICCG}, especially for the values at 30 g L^{-1} substrate loading, indicating that the adsorption capacity of TurboPETase at the attack sites on the PET surface was not impaired. It's noteworthy that TurboPETase exhibited a 3.3-fold increase in maximal reaction velocity per available reactive site ($^{inv}V_{max}/S_0$) compared with BhrPETase and LCC^{ICCG}. Since no substantial differences in $^{inv}K_M$ values were observed between TurboPETase and its parental enzymes BhrPETase and LCC^{ICCG}, we presumed that this behaviour should rely, at least in part, on the ability to attack a large subset of specific attack sites that can be hydrolysed to form a productive complex.

Table 1. Kinetic parameters of TurboPETase, BhrPETase, and LCC^{ICCG} derived from the inverse Michaelis–Menten experiments.

Parameters	$^{inv}K_M$ (mg_{enzyme} g_{PET}^{-1})			$^{inv}V_{max}/S$ (μmol g^{-1} s^{-1})		
	Substrate loading					
	12 g L^{-1}	20 g L^{-1}	30 g L^{-1}	12 g L^{-1}	20 g L^{-1}	30 g L^{-1}
TurboPETase	0.40±0.11	0.33±0.05	0.16±0.02	0.087±0.004	0.094±0.002	0.078±0.001
BhrPETase	0.52±0.19	0.26±0.11	0.18±0.03	0.026±0.002	0.028±0.002	0.025±0.001
LCC^{ICCG}	0.35±0.03	0.28±0.12	0.16±0.02	0.023±0.001	0.026±0.001	0.024±0.001

According to the model of TurboPETase predicted by AlphaFold2 and subsequent molecular dynamics (MD) simulations, key aspects of the improved performance of TurboPETase were proposed as follows: improved flexibility of the substrate binding cleft (H218S/F222I, W104L and F243T), optimized charge–charge interactions at the protein surface (A209R and D238K), and introduction of a disulfide bond (A251C-A281C). A209R, D238K, and the disulfide bond A251C-A281C are suggested to primarily contribute to improving thermostability while maintaining activity (Supplementary Fig. S3), whereas the enhanced hydrolysis efficacy may be attributed to substitutions in proximity to the active sites. Chen *et al.* found that PET hydrolytic activity could benefit from the higher flexibility of the active site in the H214S/F218F double mutant [30]. This trend was maintained by the synergistic interactions conferred by the addition of W104L and F243T, as revealed by the Cα root-mean-square fluctuation (RMSF) results (Fig. 3C). The greatly increased flexibility along the PET-binding groove was suggested to provide more space to accommodate a variety of attack conformations

through dynamic binding, which may be crucial for the formation of catalytically competent complexes on different surface structures (Fig. 3D). Based on the above results, we reasoned that TurboPETase is probably more promiscuous with respect to the conformation of the PET strand it attacks. Nevertheless, detailed analysis of the mechanism requires further efforts through more in-depth research.

Complete degradation of postconsumer PET products at a large scale

Beyond the model substrates, we collected and determined the crystallinity of 19 raw, untreated postconsumer PET products used in the packaging of food, beverages, office supplies, and household goods available at local grocery store chains (Supplementary Fig. S4). Previous studies indicated that PET containers with less than 10% crystallinity could be fully degraded by PET hydrolases in 1 week, whereas a high degree of crystallinity above 20% of PET bottles and fibres led to a considerably low enzymatic degradation rate[14, 18]. In the present study, all PET samples with less than 15% crystallinity from 10 untreated postconsumer PET food containers were fully degraded by TurboPETase in merely one day (Fig. 4A and Supplementary Fig. S5). Depolymerization of a complete untreated postconsumer PET container (roughly 5.5 g with 10.5 cm length, 10.5 cm width, 3.5 cm height) was further performed by TurboPETase at 2 mg_{enzyme} g_{PET}^{-1} at 65 °C. The time-course depolymerization analysis revealed an almost linear rate during the first 12 h, and a subsequent linear decay rate was observed, with full degradation accomplished in 18 h (Fig. 4B).

Despite the PET containers, which can be biodegraded *in situ* without any treatment, we evaluated the performance of TurboPETase on 9 untreated PET products with crystallinity above 20%. Unfortunately, a maximum depolymerization of 4% was reached within 24 h, with the levels of subsequent degradation products not increasing over time (Supplementary Fig. S6). The addition of fresh enzymes did not give rise to any additional products, suggesting that the reaction was not halted by catalyst deactivation. These results were consistent with a previous suggestion that crystallinity might be the most important factor that influences enzymatic degradation[20]. Therefore, for industrial-scale biocatalytic recycling of highly crystalline PET products, pretreatment by thermomechanical amorphization is essential for providing uniformly degradable substrates. We further explored the scale-up depolymerization of 200 g L^{-1} and 300 g L^{-1} postconsumer coloured PET bottle wastes to evaluate the maximal reactor productivity. A melt-quenching pretreatment of the highly crystalline PET materials was applied accordingly to amorphize and increase the number of surface attack sites. To our delight, nearly complete depolymerization of postconsumer coloured PET bottle wastes was achieved in 8 h and 10 h for substrate loading levels of 200 g L^{-1} and 300 g L^{-1} at 2 mg_{enzyme} g_{PET}^{-1} at 65 °C, respectively (Fig. 4C). The results demonstrate a significantly higher depolymerization performance of TurboPETase at 65 °C relative to LCC^{ICCG} at elevated temperatures, and highlight the suppression of the “physical aging” process to eliminate the 10% conversion loss. In addition to the achieved full degradation with almost no residual PET waste, the successful implementation at 300 g L^{-1} substrate loading in the present study rendered a scale-up production feasible, which may impact an approximately 20% decrease in the minimum selling price (MSP) of recycled TPA (from $2.25/kg to $1.78/kg), whereas the total enzyme

cost only accounts for 6% of the overall MSP[15]. The initial rate achieved a maximum productivity of 77.3 $g_{TPAeq.}$ L^{-1} h^{-1}, which was 1.8-fold higher than the productivity reported previously by using LCC^{ICCG} with postconsumer coloured-flake PET waste[13]. Degradation at higher substrate loading levels was also evaluated, exhibiting unsacrificed enzymatic performance but compromised hydrolysis efficiency due to the precipitation of supersaturated TPA monomers.

Encouraged by the superior degradation performance of TurboPETase, we subsequently attempted to deconstruct lower-grade PET products made from recycled PET bottle flakes. Large scale depolymerization of coloured strappings at 300 g L^{-1} substrate loading also led to ~100% conversion in 16 h, with a maximum productivity of 66.3 $g_{TPAeq.}$ L^{-1} h^{-1} (Fig. 4D). The PET strapping powders after sieving were more inhomogeneous than the PET bottle powders due to their higher hardness. Since the particle size can influence the biocatalytic degradability of PET, it may partly explain the hysteresis of the depolymerization of PET strapping. Although recycled PET recovered from bottles can be used in other lower-grade PET applications, postconsumer lower-grade products can no longer be recycled via mechanical recycling and will thus ultimately find its way to accumulate in the environment[40]. Complete degradation of the lower-grade PET products with TurboPETase at a high industrially relevant scale provides a potential route for full circularity of PET materials.

Discussion

Biocatalytic PET depolymerization represents a sustainable, low-energy solution to PET recycling, especially compared with current disposal routes such as landfills and incineration. Despite significant progress made by recent research efforts to this end, the fact that only partial depolymerization is achieved due to the low biodegradability of the remaining PET waste continues to pose a challenge. Although the chain mobility of PET increases at elevated temperatures close to the glass transition temperature (T_g) of PET, physical aging of PET can gradually convert the amorphous fraction to crystalline microstructures with limited accessibility to enzymatic hydrolysis. Therefore, using biocatalysts with only high thermostability is insufficient for eliminating the conversion loss. The main challenge lies in identifying efficient PET hydrolases with balanced thermostability and high depolymerization capability, aiming to not only reduce the biorecycling process cost but also overcome the competitive physical aging process that accompanies enzymatic degradation.

Recent protein engineering studies and more than 70 crystal structures of bacterial PET-degrading enzymes have improved our understanding of the enzymatic degradation process. However, this has not been accompanied by parallel biochemical investigations, especially for some studies that confounded the hydrolytic activities with end-point concentrations during long contact periods. Although this tendency has been rectified in recent reports, evaluation of the depolymerization performance of interfacial enzymes remains ambiguous, mainly due to the lack of consideration of the interfacial reaction characteristics. The number of real attack sites are not consistent with the total substrate loading levels, which makes the Michaelis–Menten equation invalid for describing the reaction mechanism. As a

consequence, depolymerases exhibit strikingly different catalytic performance at various enzyme concentrations, which can explain the insufficient hydrolytic ability of the currently reported PET hydrolases under enzyme saturation conditions. Although some enzymes have outstanding hydrolytic performance under certain conditions (including using specific substrates, such as oligomeric PET, at low temperatures, at different enzyme concentrations, and with additives), further engineering efforts should evaluate their hydrolytic efficiency under industrially relevant conditions to assess their potential for real scenarios. Furthermore, the MD simulations and kinetic analyses derived from an inverse Michaelis–Menten reaction regime in the present study reveal important discoveries for improving the catalytic performance of TurboPETase, demonstrating a future focus of enzyme design to improve the specific polymer interactions on attack sites rather than the general nonspecific surface adsorption. This is typically difficult to address rationally, providing room for machine-learning methods to uncover hidden information regarding the improvement of polymer degradation during the evolution of esterase. The hydrolytic activity of the predicted active mutation (W104L) in other PET hydrolases was notably higher than their respective scaffolds, encouragingly demonstrating the portability of the machine-learning-predicted mutation. With the accumulation of more experimental information and structural models generated by AlphaFold, this approach may serve as a good option for the engineering of interfacial enzymes.

In summary, this study presents a computational redesign of a PET hydrolase that significantly outperforms other PET hydrolases to address the challenge with regard to the last 10% residual nonbiodegradable PET waste. The *in silico* engineering strategy and the interfacial reaction schemes have improved the feasibility of engineering efficient PET hydrolases for industrial applications and may continue to underpin future efforts to design efficient plastic-degrading enzymes to address the challenges associated with other more abundant plastics, such as polyurethanes with hydrolysable backbones.

Declarations

Acknowledgements

This work was supported by the National Key R&D Program of China (grant no. 2018YFA0901600, 2021YFC2103600), the National Natural Science Foundation of China (31822002 and 32170033), the Key Research Program of Frontier Sciences (ZDBS-LY-SM014), the Biological Resources Program (KFJ-BRP-009 and KFJ-BRP-017-58) from the Chinese Academy of Sciences, the Informatization Plan of Chinese Academy of Sciences (CAS-WX2021SF-0111), and the Youth Innovation Promotion Association CAS (2022086).

Author contributions

B.W. initiated the project. Y.L.C. and J.Y.S. performed the computational work, Y.C.C., H.P., Z.H.C. and C.L.L. performed biochemical and biocatalytic experiments, T.Z and W.C.G. performed polymer

degradation experiments, Y.L.C and B.W. drafted the manuscript, which was revised and approved by all authors.

Competing interests

Authors declare no competing interests.

References

1. Geyer, R., Jambeck, J. R. & Law, K. L. Production, use, and fate of all plastics ever made. *Sci. Adv.* **3,** e1700782 (2017).
2. Plastics - the facts 2021 • plastics Europe. *Plastics Europe* (2022). Available at: https://plasticseurope.org/knowledge-hub/plastics-the-facts-2021/. (Accessed: 5th January 2023)
3. Jambeck, J. R. et al. Plastic waste inputs from land into the ocean. *Science* **347**, 768-771 (2015).
4. Santos, R. G., Machovsky-Capuska, G. E. & Andrades, R. Plastic ingestion as an evolutionary trap: Toward a holistic understanding. *Science* **373**, 56-60 (2021).
5. MacLeod, M., Arp, H. P. H., Tekman, M. B. & Jahnke, A. The global threat from plastic pollution. *Science* **373**, 61-65 (2021).
6. Simon, N. et al. A binding global agreement to address the life cycle of plastics. *Science* **373**, 43-47 (2021).
7. Narancic, T. et al. Biodegradable plastic blends create new possibilities for end-of-life management of plastics but they are not a panacea for plastic pollution. *Environ. Sci. Technol.* **52**, 10441-10452 (2018).
8. Ellis, L. D. et al. Chemical and biological catalysis for plastics recycling and upcycling. *Nat. Catal.* **4**, 539-556 (2021).
9. Kakadellis, S. & Rosetto, G. Achieving a circular bioeconomy for plastics. *Science* **373**, 49-50 (2021).
10. Wei, R. et al. Possibilities and limitations of biotechnological plastic degradation and recycling. *Nat. Catal.* **3**, 867-871 (2020).
11. Taniguchi, I. et al. Biodegradation of PET: current status and application aspects. *ACS Catal.* **9**, 4089-4105 (2019).
12. Wei, R. *et al.* Mechanism-based design of efficient PET hydrolases. *ACS Catal.* **12**, 3382-3396 (2022).
13. Tournier, V. et al. An engineered PET depolymerase to break down and recycle plastic bottles. *Nature* **580**, 216–219 (2020).
14. Wei, R. *et al.* Biocatalytic degradation efficiency of postconsumer polyethylene terephthalate packaging determined by their polymer microstructures. *Adv. Sci.* **6**, 1900491 (2019).
15. Singh, A. *et al.* Techno-economic, life-cycle, and socioeconomic impact analysis of enzymatic recycling of poly(ethylene terephthalate). *Joule* **5**, 2479-2503 (2021).

16. Kari, J., Andersen, M., Borch, K. & Westh, P. An inverse Michaelis–Menten approach for interfacial enzyme kinetics. *ACS Catal.* **7**, 4904-4914 (2017).
17. Baath, J. A., Borch, K., Jensen, K., Brask, J. & Westh, P. Comparative biochemistry of four polyester (PET) hydrolases. *ChemBioChem* **22**, 1627-1637 (2021).
18. Lu, H. *et al.* Machine learning-aided engineering of hydrolases for PET depolymerization. *Nature* **604**, 662-667 (2022).
19. Bell, E. L. *et al.* Directed evolution of an efficient and thermostable PET depolymerase. *Nat. Catal.* **5**, 673-681 (2022).
20. Pfaff, L. *et al.* Multiple substrate binding mode-guided engineering of a thermophilic PET hydrolase. *ACS Catal.* **12**, 9790-9800 (2022).
21. Cui, Y. *et al.* Computational redesign of a PETase for plastic biodegradation under ambient condition by the GRAPE strategy. *ACS Catal.* **11**, 1340-1350 (2021).
22. Xi, X. *et al.* Secretory expression in *Bacillus subtilis* and biochemical characterization of a highly thermostable polyethylene terephthalate hydrolase from bacterium HR29. *Enzyme Microb. Technol.* **143**, 109715 (2021).
23. Erickson, E. *et al.* Comparative performance of PETase as a function of reaction conditions, substrate properties, and product accumulation. *ChemSusChem* **15**, e202101932 (2022).
24. Cui, Y., Sun, J. & Wu, B. Computational enzyme redesign: large jumps in function. *Trends Chem.* **4**, 409-419 (2022).
25. Boneta, S., Arafet, K. & Moliner, V. QM/MM study of the enzymatic biodegradation mechanism of polyethylene terephthalate. *J. Chem. Inf. Model.* **61**, 3041-3051 (2021).
26. Ding, X., Zou, Z. & Brooks Iii, C. L. Deciphering protein evolution and fitness landscapes with latent space models. *Nat. Commun.* **10**, 5644 (2019).
27. Alley, E. C., Khimulya, G., Biswas, S., AlQuraishi, M. & Church, G. M. Unified rational protein engineering with sequence-based deep representation learning. *Nat. Methods* **16**, 1315-1322 (2019).
28. Biswas, S., Khimulya, G., Alley, E. C., Esvelt, K. M. & Church, G. M. Low-N protein engineering with data-efficient deep learning. *Nat. Methods* **18**, 389-396 (2021).
29. Zeng, W. *et al.* Substrate-binding mode of a thermophilic PET hydrolase and engineering the enzyme to enhance the hydrolytic efficacy. *ACS Catal.* **12**, 3033-3040 (2022).
30. Chen, C.-C. *et al.* General features to enhance enzymatic activity of poly(ethylene terephthalate) hydrolysis. *Nat. Catal.* **4**, 425-430, (2021).
31. Delgado, J., Radusky, L. G., Cianferoni, D. & Serrano, L. FoldX 5.0: working with RNA, small molecules and a new graphical interface. *Bioinformatics* **35**, 4168-4169 (2019).
32. Park, H. *et al.* Simultaneous optimization of biomolecular energy functions on features from small molecules and macromolecules. *J. Chem. Theory Comput.* **12**, 6201-6212 (2016).
33. Xiong, P. *et al.* Protein design with a comprehensive statistical energy function and boosted by experimental selection for foldability. *Nat. Commun.* **5**, 5330 (2014).

34. Arabnejad, H. *et al.* A robust cosolvent-compatible halohydrin dehalogenase by computational library design. *Protein Eng. Des. Sel.* **30**, 173-187 (2017).
35. Müller, R.-J., Schrader, H., Profe, J., Dresler, K. & Deckwer, W.-D. Enzymatic degradation of poly(ethylene terephthalate): rapid hydrolyse using a hydrolase from *T. fusca*. *Macromol. Rapid Commun.* **26**, 1400-1405 (2005).
36. Then, J. *et al.* Ca^{2+} and Mg^{2+} binding site engineering increases the degradation of polyethylene terephthalate films by polyester hydrolases from *Thermobifida fusca*. *Biotechnol. J.* **10**, 592-598 (2015).
37. Schiano-di-Cola, C. *et al.* Systematic deletions in the cellobiohydrolase (CBH) Cel7A from the fungus *Trichoderma reesei* reveal flexible loops critical for CBH activity. *J. Biol. Chem.* **294**, 1807-1815 (2019).
38. Schiano-di-Cola, C. *et al.* Structural and biochemical characterization of a family 7 highly thermostable endoglucanase from the fungus *Rasamsonia emersonii*. *FEBS J.* **287**, 2577-2596 (2020).
39. Badino, S. F., Kari, J., Christensen, S. J., Borch, K. & Westh, P. Direct kinetic comparison of the two cellobiohydrolases Cel6A and Cel7A from *Hypocrea jecorina*. *Biochim. Biophys. Acta Proteins Proteom.* **1865**, 1739-1745 (2017).
40. Lamberti, F. M., Román-Ramírez, L. A. & Wood, J. Recycling of bioplastics: routes and benefits. *J. Polym. Environ.* **28**, 2551-2571 (2020).

Figures

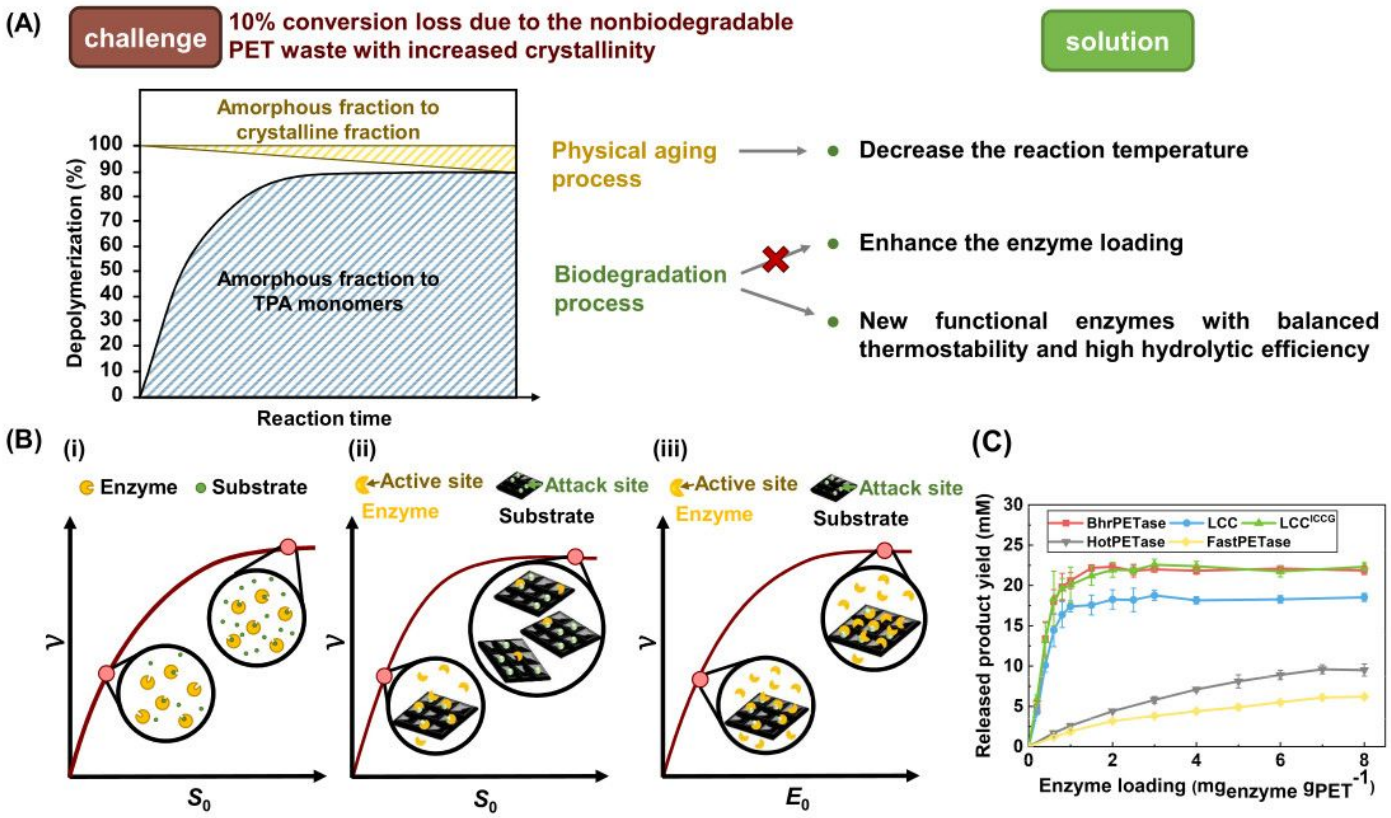

Figure 1

(A) The current challenges and solutions for the PET biodegradation process. (B) Simplified illustration of (i) homogeneous enzyme kinetics with soluble enzymes and substrates, and (ii, iii) heterogeneous enzyme kinetics of soluble enzymes acting on insoluble substrates. The red curve is a plot of the initial reaction rate, *v*, against the total concentration of substrate (S_0) or enzyme (E_0). At high substrate loads (ii), the entire enzyme population is engaged in complexation (as in traditional Michaelis–Menten saturation). Conversely, at high enzyme loads (iii), all attack sites are complexed with the enzyme. (C) Comparison of PET hydrolase activity at different enzyme loading levels towards the formation of an amorphous PET film (Gf-PET, from the supplier Goodfellow, substrate loading 30 g L^{-1}). Reactions were performed in 1 M potassium phosphate buffer (pH 8.0) for 6 h at 50 °C for FastPETase and 65 °C for other PET hydrolases. All measurements were conducted in triplicate (n = 3).

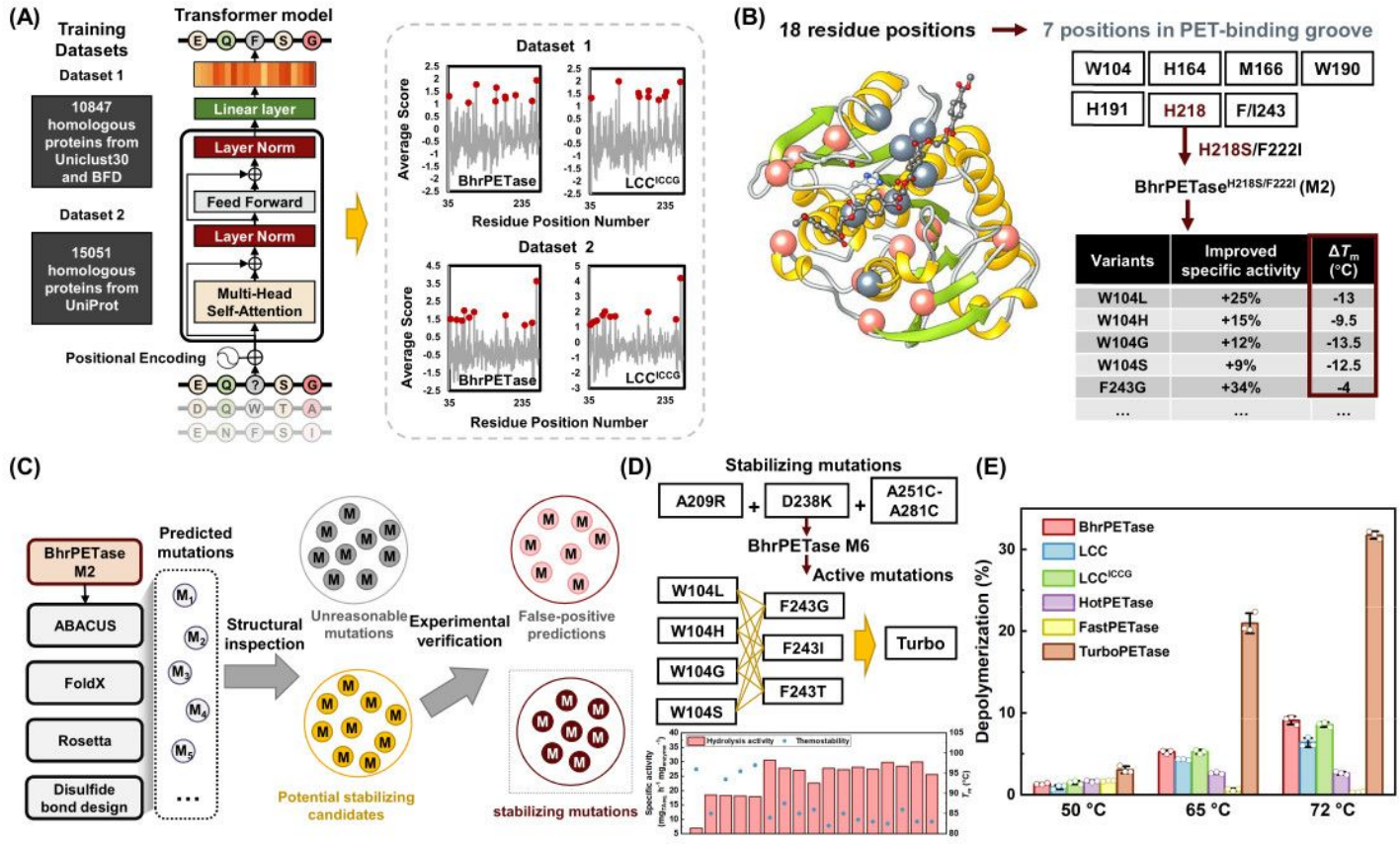

Figure 2

Schematic representation of the redesign of PET hydrolases using the hybrid computational method. (A) Potentially beneficial mutations are predicted with the Transformer model trained on two datasets. The top ten predicted amino acid positions (red circles) were selected. Removal of duplicate positions resulted in 18 residue positions. (B) Locations of the 18 residue positions in the structural model of the BhrPETase-PET complex (left panel). Among the 18 predicted positions, 7 positions were suggested to be located at the PET binding site. The Cα atoms of these amino acid positions are shown as dark blue spheres, whereas the 11 remaining positions are shown as coral spheres. PET and the catalytic triad are shown as ball-and-stick representations. The previously reported H218S/F222I variant was initially added to BhrPETase (right panel). Adding the variants at the remaining 6 positions to the BhrPETase$^{H218S/F222I}$ (BhrPETase M2) variant led to dramatically decreased stability. (C) Potentially stabilizing mutations were predicted by the GRAPE strategy based on the predicted structural model of the BhrPETase M2 variant. (D) Accumulation of beneficial mutations. Stabilizing mutations were initially added to the BhrPETase M2 variant, which resulted in the thermostable variant BhrPETase M6. The active mutations at the W104 and F243 positions were combinatorically assembled and accumulated in the BhrPETase M6 variant. The bar chart and the scatter represent the specific activity and thermostability of the wild type and its variants,

respectively. (E) Comparison of the depolymerization of amorphous Gf-PET films with PET hydrolases under enzyme saturation conditions at reaction temperatures ranging from 50 to 72 °C. The bar chart shows the mean depolymerization after 3 h of reaction. The enzyme loading levels were as follows: BhrPETase, LCC, LCC^{ICCG}, and TurboPETase, 2 mg_{enzyme} g_{PET}^{-1}; HotPETase and FastPETase, 7 mg_{enzyme} g_{PET}^{-1}. All measurements were conducted in triplicate (n = 3).

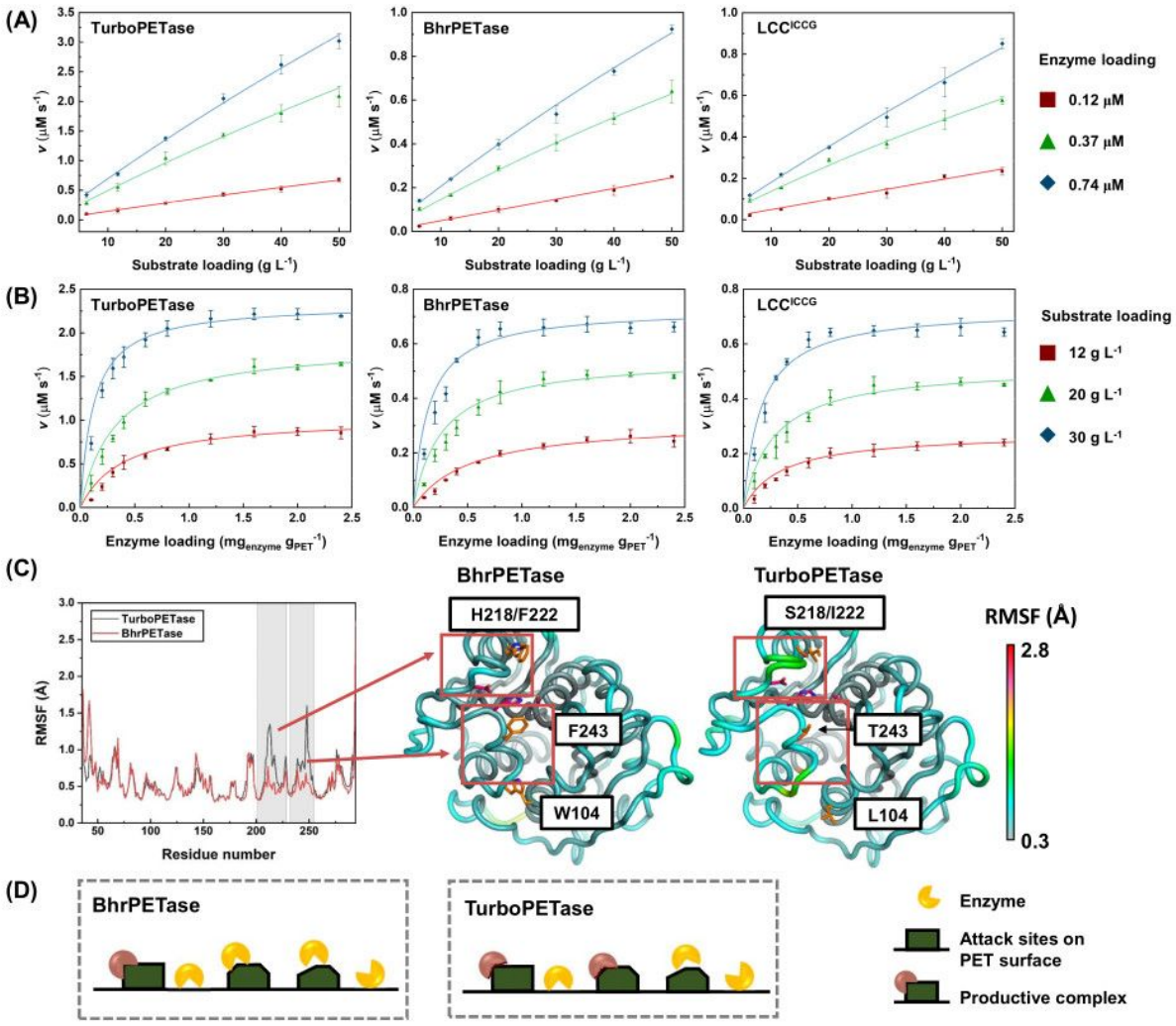

Figure 3

(A) Conventional and (B) inverse Michaelis–Menten plots of TurboPETase, BhrPETase, and LCC^{ICCG} at 65 °C. Error bars represent the standard deviation of reactions performed in triplicate. (C) RMSF values (in Å) for all Cα atoms of BhrPETase and TurboPETase during the MD simulations, indicating global changes in protein flexibility, especially for the PET-binding groove. The H218S/F222I, W104L and F243T mutations are shown as orange atoms, whereas the catalytic triad is shown as hot pink atoms. (D) Schematic diagram of PET depolymerization processes. TurboPETase may be more promiscuous than the wild-type enzyme due to the increased flexibility along the protein PET-binding groove, which allows it to attack different surface structures.

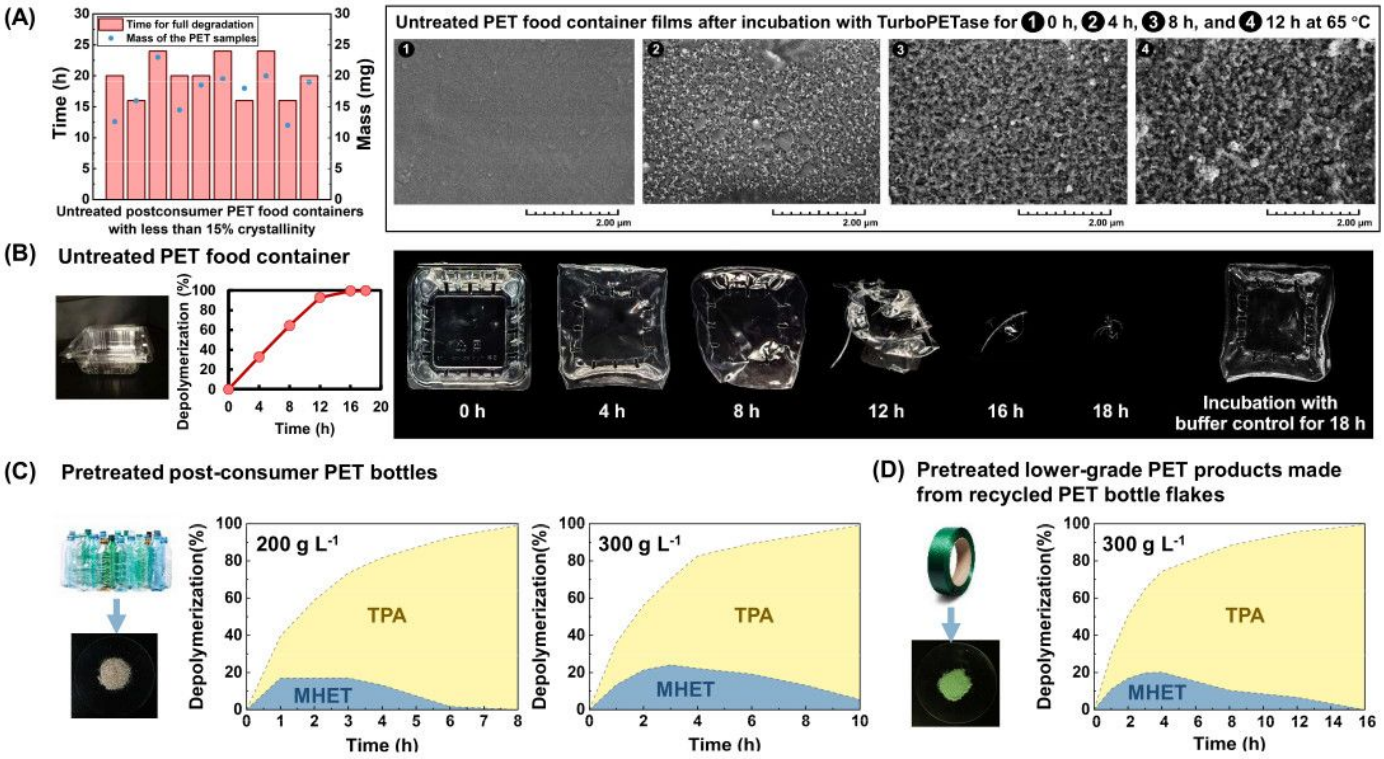

Figure 4

(A) Complete depolymerization of the untreated PET container films (⌀8 mm, 12-23 mg) with less than 15% crystallinity with TurboPETase (left panel) and the SEM images for depolymerization of untreated PET film (⌀8 mm, 16 mg) from food container H125B following various exposure times (right panel). All measurements were conducted in triplicate (n = 3). (B) Time course of the degradation of a large, untreated PET container (roughly 5.5 g) with TurboPETase. (C) Nearly complete degradation of pretreated PET bottles at 200 g L^{-1} and 300 g L^{-1} solid loading levels. (D) Nearly complete degradation of pretreated PET coloured strapping at 300 g L^{-1} solid loading. All reactions were performed at 65 °C with 2 mg_{enzyme} g_{PET}^{-1} enzyme loading.

Supplementary Files

This is a list of supplementary files associated with this preprint. Click to download.

- SI.pdf